AMERICAN SCIENTIFIC PUBLISHERS

Science of Advanced Materials
Vol. 10, pp. 937–949, 2018
www.aspbs.com/sam

ARTICLE

Potassium Hydroxide Activated and Nitrogen Doped Graphene with Enhanced Supercapacitive Behavior

Weiyuan Deng[1], Tianhe Kang[1,*], Hu Liu[2,3], Jiaoxia Zhang[2,4], Ning Wang[5], Na Lu[6], Yong Ma[2,7], Ahmad Umar[8,*], and Zhanhu Guo[2,*]

[1]*Institute of Mining Technology, Taiyuan University of Technology, Taiyuan 030024, China*
[2]*Integrated Composites Laboratory (ICL), Department of Chemical and Biomolecular Engineering, University of Tennessee, Knoxville, TN 37996, USA*
[3]*National Engineering Research Center for Advanced Polymer Processing Technology, Zhengzhou University, Zhengzhou 450002, China*
[4]*School of Material Science and Engineering, Jiangsu University of Science and Technology (JUST), Zhenjiang, Jiangsu 212003, China*
[5]*State Key Laboratory of Marine Resource Utilization in South China Sea, Hainan University, Haikou 570228, P. R. China*
[6]*Lyles School of Civil Engineering, School of Materials Engineering, Birck Nanotechnology Center, Purdue University, West Lafayette, 47906, USA*
[7]*College of Materials Science and Engineering, Shandong University of Science and Technology, Qingdao 266590, China*
[8]*Department of Chemistry, Faculty of Sciences and Arts and Promising Centre for Sensors and Electronic Devices (PCSED), Najran University, Najran, 11001, Saudi Arabia*

ABSTRACT

For the goal of synthesizing high performance supercapacitor electrode materials to meet the pressing requirements of energy storage, a facile hydrothermal method was employed to prepare nitrogen doped activated graphene (N-AG), two steps, i.e., KOH activating and following nitrogen doping were performed using a hydrothermal method. Continuously increased I_D/I_G ratios were observed in the Raman spectra after KOH activation and following N-doping processes, indicating increased defects due to the etching effect of KOH and introduced nitrogen defects on graphene sheet. Stacked graphene with damaged sheets on the surface was clearly seen in TEM image after the KOH etching. The successful dopant of N was demonstrated by XPS spectra and EDS mapping, confirming the effective hydrothermal N doping method. The N-AG exhibited largely enhanced capacitance (186.63 F/g) and cycling stability compared with that of nitrogen doped graphene (N-G, 50.88 F/g) and activated graphene (AG, 58.38 F/g) due to the combined positive effects of KOH activation and N-doping.

KEYWORDS: Graphene, KOH Activation, Nitrogen Doping, Enhanced Capacitance, Supercapacitor.

1. INTRODUCTION

Electrochemical storage devices with high energy and power density are highly desired with the fast-growing market for portable electronics, hybrid electric vehicles and stand-by power systems.[1–7] Due to their high power densities, fast charging/discharging rate, sustainable cycling life and excellent cycle stability, ultracapacitors based on electrostatic interactions between ions in the electrolyte and electrodes, occurring in so-called electrical double layers (EDLs) are widely explored and become a promising technique to utilize the intermittent renewable energy.[8–12] Different carbon nanomaterials such as activated carbon,[13,14] carbon black,[15] carbon onions,[16] carbon nanotubes[17–21] and carbon nanofibers[22–24] have been widely employed for electrode materials of ultracapacitors due to their high specific surface area and electrical conductivity. However, pure carbon materials based ultracapacitors always exhibit low capacitance which largely limits their applications to complementary energy storage devices to batteries.[25,26] In order to resolve the insufficient capacitance issue, another class of capacitors as pseudocapacitors were developed, which employed metal oxides,[27–30] and conducting polymers[31–37] to store electrical energy based on the redox reaction near the surfaces of those active materials.[36,38] However, the poor cycle lives of most pseudocapacitors are the main limitations as the redox reactions are not fully reversible and also accompanied with the expansion-constrain of electrode.[39–41] In this case, the strategy of introducing pseudocapacitance properties to the electrode materials of

*Authors to whom correspondence should be addressed.
Emails: kangtianhe@163.com, ahmadumar786@gmail.com, zguo10@utk.edu
Received: 24 September 2017
Accepted: 18 January 2018

ARTICLE

ultracapacitors is a vital candidate since they can not only exhibit comparable capacitances to those of pseudocapacitors but also still utilize the robust charging mechanisms of ultracapacitors and hence exhibiting excellent cycle lives.[22, 42, 43]

Among all the carbon materials, graphene with an atom-thick two dimensional (2D) carbon structures has attracted great attention due to its unique electrical, chemical, thermal, and mechanical properties.[3, 13, 18, 44–59]

Nowadays, in order to advance its various potential applications such as nanoelectronics, energy storage/conversion, and catalysis,[60–65] dramatic scientific endeavors have been launched toward the optimization of by manipulating its electronic mechanical, chemical and structural properties.[19, 66–70] Reconstructed graphene could potentially result in localized highly reactive regions and thus unexpected properties,[71, 72] i.e., enrich reactive oxygen functional groups on graphene sheets can provide ample covalent bonding sites for the chemical functionalization.[73, 74] In addition, introducing heteroatoms into the carbon frameworks is another effective way to improve the specific performances of graphene.[75, 76] It has been reported that certain heteroatoms (B, S, N and P) dopant seems to be the most promising choice for enhancing capacity, surface wettability and electronic conductivity of graphene while maintaining the superb cycle ability.[77–80] Among them, Nitrogen (N)-doped carbon has been extensively investigated recently, it exhibits excellent performance in oxygen reduction reaction (ORR) and lithium ion battery due to the unique electronic interactions between the lone-pair of nitrogen and the π-system of graphic carbon.[81, 82] Nowadays, two approaches as post-treatment in N-environment and *in-situ* doping using N-containing precursors are mainly employed to achieve this goal.[83] However, their complicated preparation procedures and high cost manipulations largely restricted the practical uses in large scale. Therefore, an easy operating method producing nitrogen doped graphene with uniform and high-concentration nitrogen is still urgently needed.

Alternatively, it is generally accepted that the capacitance and power capability of the carbon materials are largely related to their electrolyte-accessible surface area and the kinetics within active materials.[84] Chemical activation has been proven as a high efficient method to obtain carbons with high surface area and narrow micropore distribution.[85–87] Among all the chemical activation agents, potassium hydroxide (KOH) as a strong alkaline is very promising due to its etching nature, negligible activation temperature, high yields, resulted well defined micropore size distribution and ultrahigh specific surface area.[86, 88] Enhanced performances of numerous kinds of carbon such as carbon black,[89] coals,[90] chars,[91] fibers,[86] nonotubes[87] and graphenes[92] have been observed after KOH activation. Furthermore, since a large amount of defects can be introduced on the graphene sheets after KOH etching, it is expecting that different nitrogen doping results will be obtained on the KOH activated graphene due to the altered mechanical structure and electron transfer pathway.

Herein, we have developed a facile hydrothermal method combining both KOH activation and N-doping processes to synthesize the nitrogen doped activated graphene (N-AG) using exfoliated graphene oxide (GO) solution as precursor. GO simply suffers N-doping and KOH activation were also synthesized as N-graphene (N-G) and porous graphene (AG) as control experiments. This reaction was carried out in a mild hydrothermal environment employing KOH and ammonia reagent as reactants. The defects variation on graphene sheets after KOH activation and N-doping is investigated by Raman spectra and X-ray photoelectron spectroscopy (XPS). The morphology of graphene is revealed by scanning electron microscopy (SEM) and transmission electron microscopy (TEM). The doped N element is confirmed by the XPS and EDS mapping images. The supercapacitive performance and kinetics comparison were proceeded by cyclic voltammetry (CV), galvanostatic charge–discharge and electrochemical impedance spectroscopy (EIS) measurements. Cycling performance was also included to evaluate the practical application.

2. EXPERIMENTAL DETAILS

2.1. Materials

Natural graphite powders were supplied by Bay Carbon Inc., USA. Potassium persulfate ($K_2S_2O_8$, ≥99.0%), phosphorus pentoxide (P_2O_5, ≥98.0%) and potassium permanganate ($KMnO_4$, ≥99.0%) were purchased from Sigma Aldrich. Potassium hydroxide (KOH, BioXtra, ≥85% KOH basis), ammonium hydroxide (NH_4OH, Assay: 28.0 to 30.0 w/w%), sulfuric acid (H_2SO_4, 93–98%), Hydrochloric acid (HCl, 37.5%) and hydrogen peroxide aqueous solution (PERDROGEN® 30% H_2O_2 (w/w)) were purchased from Alfa Aesar. The dialysis membrane (Spectra/Por, molecular weight cut off (MWCO): 12000–14000) was commercially obtained from Spectrum Laboratories, Inc. All the materials were used as received without any further treatment.

2.2. Synthesis Method

Graphite oxide (GO) was synthesized following the modified Hummers method.[76–93] For the synthesis of nitrogen doped graphene (N-G) and KOH activated graphene (AG), 26.0 g homogeneous GO solution (0.338 g GO) was first transferred to a 40 ml teflon lined hydrothermal autoclave, 3 ml NH_4OH solution or well dissolved KOH solution (4.05 g KOH, mass KOH:GO = 12:1) was following added, the solution was diluted to 40 ml and sealed maintained at 150 °C for 3 hrs. After cooling down, the precipitates were collected by filtration and washed with water for 3 times, the products were dried naturally for 72 hours. Reduced graphene oxide (RGO) was also obtained following the same procedure using simple origin

GO solutions as a control experiment. For the synthesis of nitrogen doped activated graphene (N-AG), 0.2 g synthesized AG powder were uniformly grinded and dissolved in 30 ml water, which undergo a 30 min sonication to achieve a uniform distribution, the AG solution was then transferred to a 40 ml autoclave added with 1.80 ml NH_4OH solution (same NH_4OH/AG ratio as that of NH_4OH/GO). Similar procedures were following proceeded to get the N-AG powder products.

2.3. Preparation of Working Electrode

Three electrode system was employed to characterize the supercapacitive property. The working glassy carbon electrode with a diameter of 3 mm was successively polished with 1.0 and 0.05 μm alumina powders on a microcloth wetted with doubly distilled water to produce an electrode with a mirror-like surface. For the preparation of sample coated electrode, 5.0 mg graphene was added to 1.0 mL ethanol solution of nafion (the content of nafion is 0.1 wt%), then the mixture was treated for 30 min with ultrasonication to form a uniform suspension. The obtained suspension (5 μL) was dropped on the surface of the well-treated glassy carbon electrode. Finally, the resultant modified glassy carbon electrode was dried naturally at room temperature.

2.4. Characterizations

Raman spectra were obtained using a Horiba Jobin-Yvon LabRam Raman confocal microscope with 785 nm laser excitation at a 1.5 cm^{-1} resolution at room temperature.

The microstructure of the sample was observed on a JEOL JEM-2100 transmission electron microscopy (TEM) and a JSM-6700F field emission scanning electron microscope (SEM).

X-ray photoelectron spectroscopy (XPS) was conducted on a Kratos Analytical spectrometer, using Al Ka = 1486.6 eV radiation as the excitation source, under a condition of anode voltage of 12 kV and an emission current of 10 mA. The element peaks were deconvoluted into the components on a Shirley background.

2.5. Electrochemical Evaluations

The electrochemical experiments were conducted in a conventional three-electrode cell. The as-prepared glassy carbon electrode deposited with active materials was used as the working electrode, platinum wire as the counter electrode, and saturated calomel electrode (SCE) (0.241 V vs. SHE) connected to the cell through a Luggin capillary serving as reference electrode. All the potentials were referred to the SCE.

Cyclic voltammogram (CV) ranging from 0 to 1.0 V at a series of scan rates and galvanostatic charge–discharge (GCD) measurements from 0 to 0.8 V with different current densities were conducted in 1.0 M H_2SO_4 aqueous solution. The electrochemical impedance spectroscopy (EIS) was carried out in the frequency range of 100,000 to 0.01 Hz with a 5 mV amplitude referring to the open circuit potential. The cycling stability was investigated through evaluating capacitance retention running 1000 galvanostatic charge–discharge cycles.

2.6. Calculations of Capacitance, Energy Density and Power Density

The capacitance of the electrodes was calculated from the corresponding CV curves at different scan rates from the corresponding CV curves at different scan rates from 0 to 1 V in 1.0 M H_2SO_4 aqueous solution using Eq. (1):

$$C_s = \left(\int idV\right) \Big/ (2m \times \Delta V \times \nu) \quad (1)$$

where C_s is the specific capacitance in F/g, $\int idV$ is the integrated area of the CV curve, m is the mass of the active materials in the single electrode in g, ΔV is the scanned potential window in V, and ν is the scan rate in V/s.

The capacitance from the GCD curves was calculated using Eq. (2):

$$C_s = (i \times t)/(m \times \Delta V) \quad (2)$$

Where C_s is the specific gravimetric capacitance in F/g, i is the discharge current in A, t is the discharge time in s, m is the mass of the active materials on the working electrode in g, and ΔV is the scanned potential window in V (excluding the IR drop at the beginning of the discharge process).

The energy density, E, and power density, P, of the electrode materials were calculated from Eqs. (3) and (4), respectively,

$$E = \frac{C_s \Delta V^2}{7.2} \quad (3)$$

$$P = \frac{3600E}{t} \quad (4)$$

where E is the specific energy density in Wh/kg, P is the specific power density in W/kg, C_s is the specific capacitance in F/g, ΔV is the scanned potential window (excluding IR drop at the beginning of the discharge process) in V, and t is the discharge time in s.

3. RESULTS AND DISCUSSION

3.1. Physical Characterizations

3.1.1. Raman Analysis

Raman spectrum is a powerful tool to characterize the crystalline structure of carbon-based materials due to their strong response to the specific electronic property. Figures 1(a)–(d) shows the Raman spectra of RGO, N-G, AG and N-AG, respectively. Similar D and G band located around 1300 and 1600 cm^{-1} are clearly seen for all the graphenes. The G band is attributed to the E_{2g} phonon

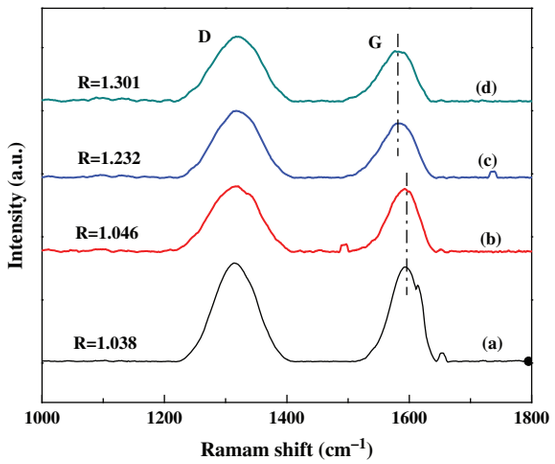

Fig. 1. Raman spectra of (a) RGO, (b) N-G, (c) AG and (d) N-AG.

mode of in-plane sp^2 carbon atoms while the D band is induced by the interruption of regular hexagonal network structure such as in-plane defects, edge defects and dangling bonds. The intensity ratio of D to G band (I_D/I_G, donated as R) is a reliable indicator to evaluate the degree of structural defects on the graphene sheets and a higher R value means more defects and disordered structure on the graphene surface.

The calculated R values are provided in Table I, It is clear obtained that the R value follows an order as N-AG (1.301) > AG (1.232) > N-G (1.046) > pure graphene (1.038), which indicates that the amount of defect is increased monotonously after N-doping and KOH activation processes, respectively. In addition, the role of KOH activation is more predominant as confirmed by the largely increased R value, indicating a greatly increase of defects or edge area on graphene sheets due to the KOH etching. Finally, an obvious negative shift of G band (from 1596 to 1581 cm^{-1}) is clearly seen after KOH activation as shown in Figures 1(c) and (d) which is probably due to the uniaxial tensile strain on graphene, indicating an reduction of GO by KOH.[95,96] The in-plane crystalline size (L_a) is also calculated using the following Eq. (1) and summarized in Table I.

$$L_a = \frac{560}{E_\lambda^4}\left(\frac{I_D}{I_G}\right)^{-1} \quad (5)$$

where E_λ is the excitation laser energy in eV used in the Raman measurement. It is clearly seen from Table I that the L_a value is inversely proportional to the R value, which indicates that the basal structure of graphene has been affected due to the introduced N containing sites and increased defects caused by KOH activation. Finally, the largely decreased L_a values of AG and N-AG are probably due to the KOH etching caused stack of graphene.

Table I. Summary of the I_D/I_G (R) and L_a values of the different graphenes.

Sample ID	R	L_a (nm)
Pure graphene	1.038	86.57
N-G	1.046	85.91
AG	1.232	72.94
N-AG	1.301	69.07

3.1.2. Morphology Characterization

The morphology variation of these four graphene was characterized by SEM as shown in Figures 2(a)–(d), TEM images were also provided inset each SEM image. It is clearly seen from Figure 2(a) that the RGO maintains a typical crumpled graphene structure, which is further confirmed by the inset TEM image. For N-G, Figure 2(b), similar morphology have been observed, indicating a negligible effect of ammonia on the morphology of RGO. However, it is clearly seen from Figure 2(c) that the graphene sheets are inclined to stack together after the KOH activation, which is probably due to the hydroxide reduction resulted decreased of oxygen containing groups on graphene sheet. In addition, a high amount of pyrolytic carbon is also noticed on their surface of graphene due to the KOH etching effect, which is further disclosed in the TEM image as a large concentration of defects are generated on the graphene surface, giving rise to increased edge area.

Furthermore, the HRTEM image at the edge of AG clearly shows the graphite layers, implying that KOH activation treatment can also induce the stacking of graphene which is consistent with the negative shift of G band in Raman. In contrast, a more fluffy structure of graphene is regained for N-AG, Figure 2(d), which is probably attributed to the sonicated process and the implanted oxygen containing groups form ammonia. However, the typical stack structure has not been changed for N-AG as confirmed by the inset TEM image. In order to further characterize the element distributions in N-AG, EDS elemental mapping characterization is also employed and displayed in Figures 2(e)–(h), uniform distributions of C (blue), O (green), K (red) and N (white) bright dots are clearly seen, indicating the well distribution of corresponding elements and this effective hydrothermal method. For the existence of K, most studies suggests that the hydroxide reduction leads to H_2 and K metals, and carbon is oxidized to carbonates according to the global reaction.[87]

$$6KOH + C \leftrightarrow 2K + 3H_2 + 2K_2CO_3$$

In addition, this successful N doping method is also confirmed by the EDS mapping images of N-G as shown in Figure 3.

3.1.3. XPS Investigation

XPS as a powerful tool investigating the composition and valence state of contained elements is also employed to characterize the structural variation of graphene as shown

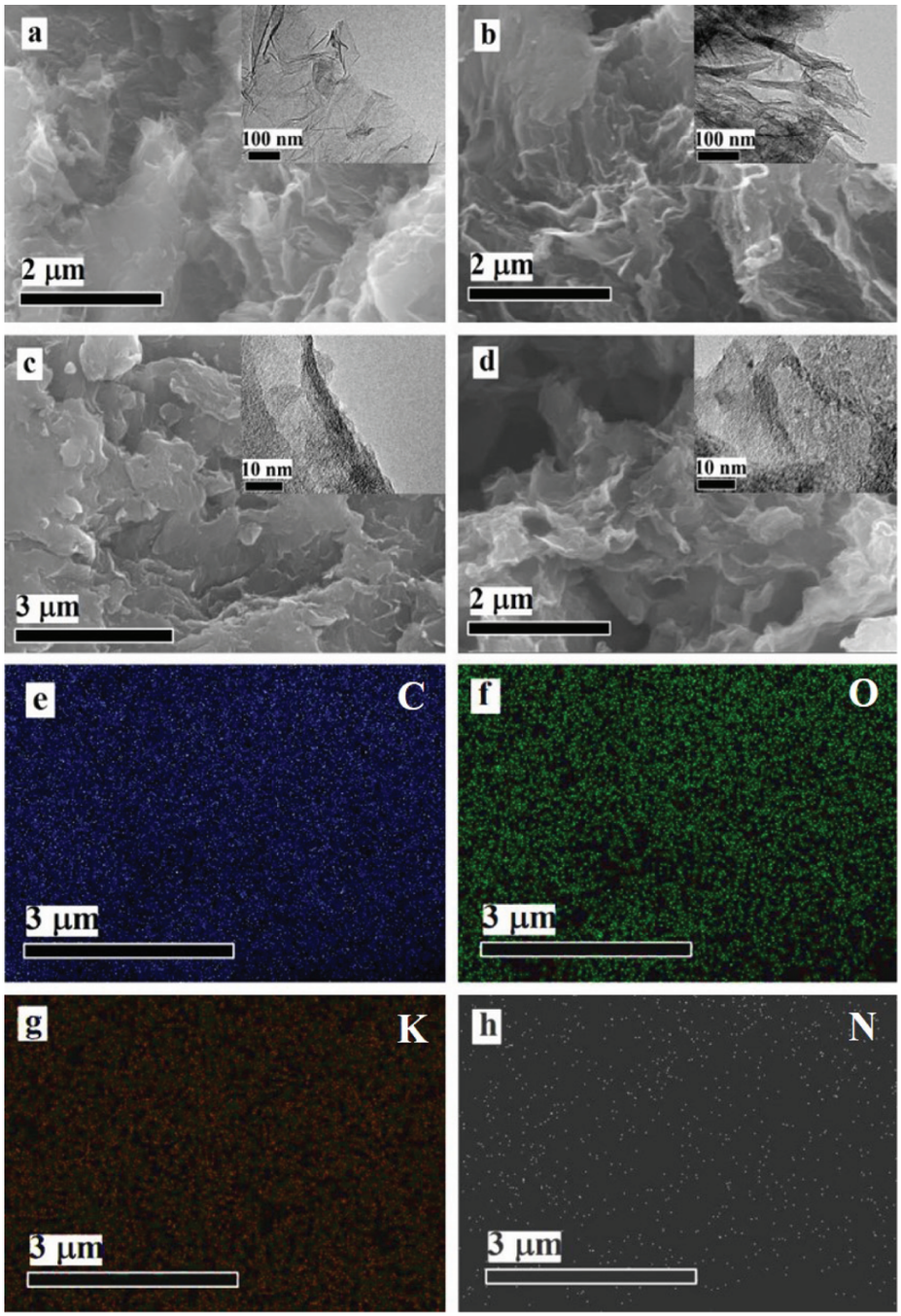

Fig. 2. SEM image of (a) RGO, (b) N-G, (c) AG and (d) N-AG, inset is the corresponding TEM image. EDX mapping image of (e) C, (f) O, (g) K and (h) N in N-AG.

in Figure 4. Figure 4(A) discloses the wide scan surveys of (a) RGO, (b) N-G, (c) AG and (d) N-AG. Common peaks as C 1*s* and O 1*s* are both seen for all these four graphene, indicating the existence of oxygen containing groups. Furthermore, for AG and N-AG, Figures (c) and (d), obvious peak assigned to K 2*s* (378 eV) and K 2*p*3 (290 eV) are also observed, indicating the containment of K which comes from the KOH precursor. In addition, for N-G and N-AG, Figures 4(b) and (d), clear peak belonging to N 1*s* is clearly seen around 400 eV, demonstrating the successful dopant of N and this effective hydrothermal method. In order to get detailed information about the dopant N, high resolution curve fitting of N is further proceeded for N-G and N-AG as shown

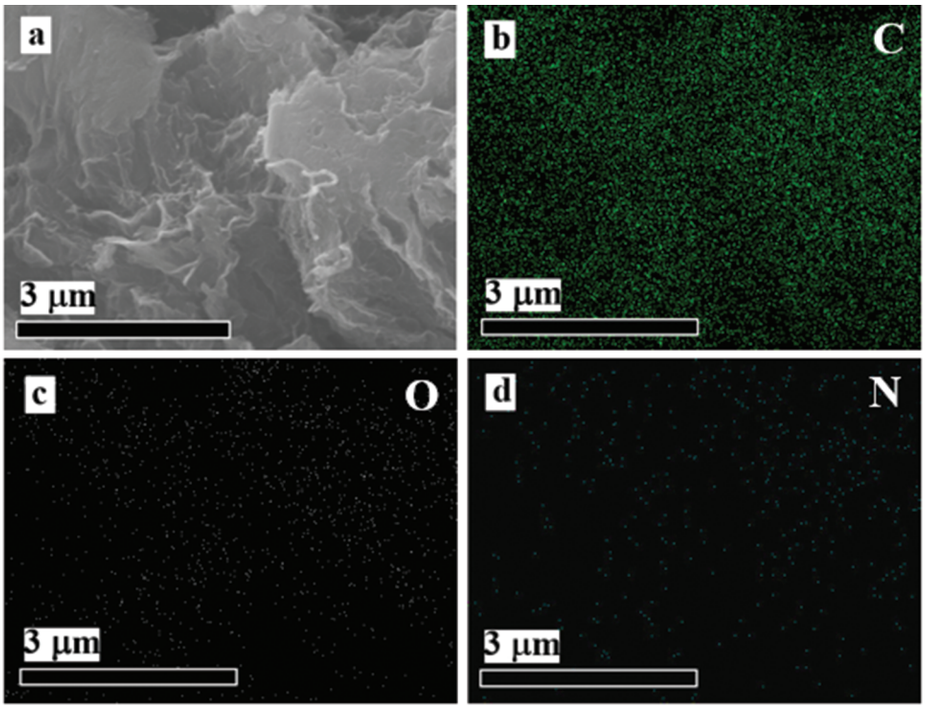

Fig. 3. (a) SEM image of NG, and corresponding EDS images of (b) C, (c), O and (d) N.

in Figure 4(B), for bottom located N-G, three peaks with binding energies at 398.6, 400.0, and 401.7 eV representing pyridinic, pyrrolic, and quaternary nitrogen are clearly obtained. Pyridinic and pyrrolic N can contribute to the increase of Fermi energy (E_f) and density of states (DOS) of graphene, while Quaternary nitrogen is described as "graphitic nitrogen" which have a p-doping effect.[96] Detaily, Pyridinic-N refers to nitrogen atoms at the edge of graphene planes, each of which is bonded to two carbon atoms and donates one *p*-electron to the aromatic π systems; pyrrolic-N refers to nitrogen atoms that are bonded to two carbon atoms and contribute to the π system with two *p*-electrons; quaternary nitrogen is also called "graphitic nitrogen" or "substituted nitrogen," in which nitrogen atoms are incorporated into the graphene layer and replace carbon atoms within a graphene plane.[97] Numerous studies have reported that the enhanced electrocatalytic activity is mainly attributed to puridinic-N and/or pyrrolic-N.[98] However, for the top N-AG, only one peak belonging to pyrrolic nitrogen is obtained, the different curve fitting results are probably due to the afore proceeded KOH activating process. For the curve fitting of C, Figures 4(C) and (D), three main groups as C–C (284.6), C–O (286.5) and C═O (288.2) are obtained for all the graphene samples, which originate from the oxidation and destruction of the sp^2 atomic structures of pristine graphene, indicating the existence of oxygen containing groups regardless of the KOH activating and N-doping processes. Figures 4(E) and (F) shows the curve fitting of O in the four graphene. The XPS spectra are fitted to get detailed chemical bonding information about the elements O with carbon. Three peaks located around 531.08, 532.03, and 533.04 eV can be assigned to the species of O_1, C═O (oxygen doubly bonded to aromatic carbon), O_2, C–OH (oxygen singly bonded to aliphatic carbon), and O_3, C–O–C/HO–C═O, respectively.[99–101] It is clearly seen from Figure 4(F) that the ratio of $(O_2+O_3)/O_1$ is largely decreased after KOH activation, which indicates a decrease of oxygen containing groups due to the hydroxide reduction and is also consistent with the TEM results about the graphene stack phenomenon. However, slight increases of O_2 and O_3 have been found for N-AG, top of Figure 3(F), indicating an increase of implanted oxygen containing groups during the reaction with ammonia.

3.2. Electrochemical Evaluations

3.2.1. Capacitance Investigation

The capacitive performances of the graphene based electrodes were studied using Cyclic voltammogram (CV) at a high scan rate of 500 mV/s within a potential range of −0.2 to 0.8 V in 1.0 M H_2SO_4 as shown in Figure 5(A), The CV curves at other scan rates (1000, 200, 100, 50 and 20 mV/s) are also provided in Figure 6. Higher current densities and larger enclosed CV areas are clearly seen in N-AG, followed by AG, N-G and RGO, indicating more energy stored in the N-AG due to the increased etched edge area and introduced N-defects. It is clearly seen from Figure 6(a) that all the RGO

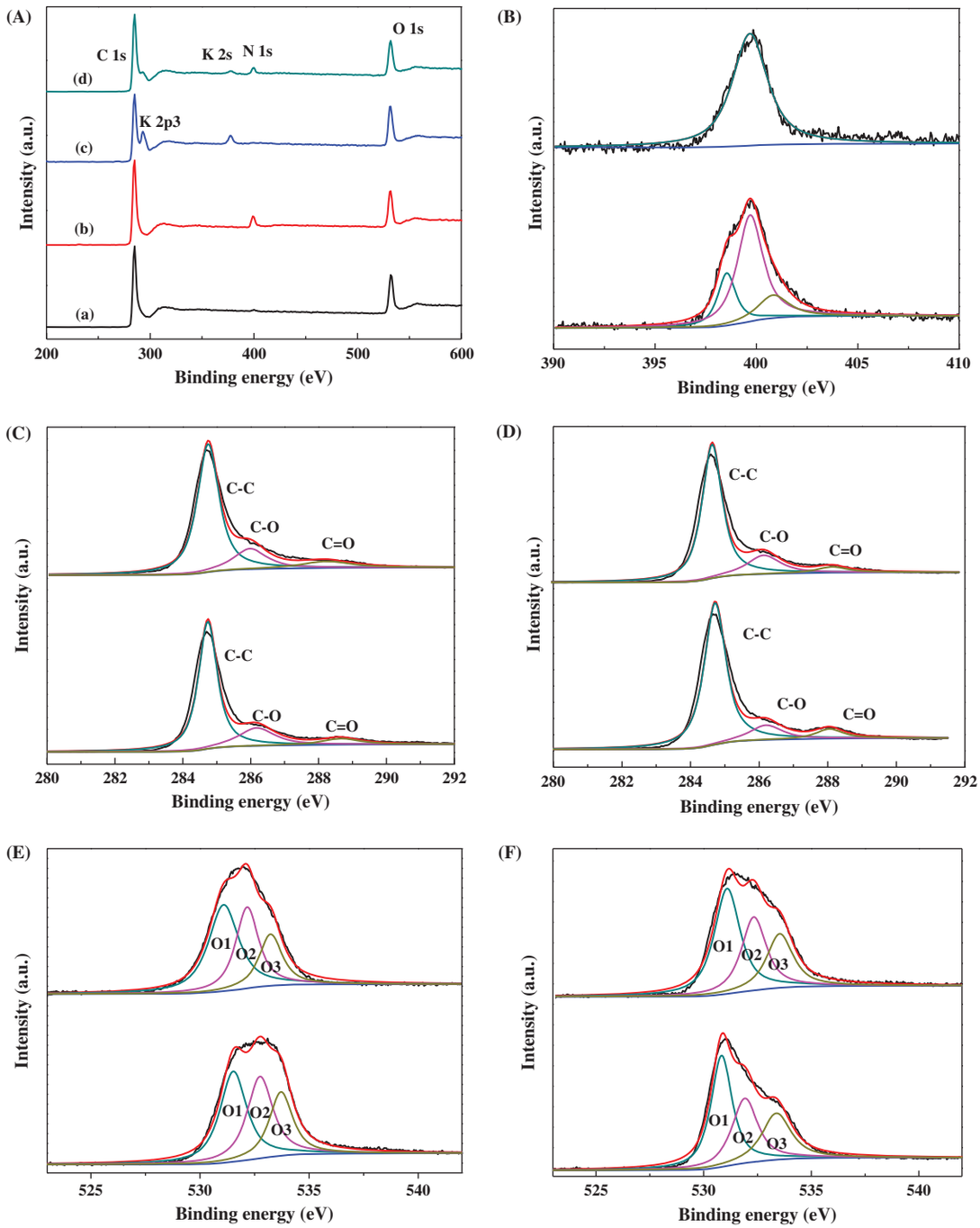

Fig. 4. XPS image as (A) wide scan survey of (a) RGO, (b) N-G, (c) AG and (d) N-AG, (B) curve fitting of N in N-G (bottom) and N-AG (top), (C) curve fitting of C in RGO (bottom) and N-G (top), (D) curve fitting of C in AG (bottom) and N-AG (top), (E) curve fitting of O in RGO (bottom) and N-G (top) and (F) curve fitting of O in AG (bottom) and N-AG (top).

exhibit nonrectangular CV curves with one obvious pair of redox peaks around 0.4/0.3 V which come from the quinine/hydroquinone redox transition, indicating the existence of oxygen-containing functionalities.[102] However, these redox peaks are largely depressed and the shape becomes more rectangular after N doping as confirmed by all the CV curves of N-G in Figure 6(b), indicating the positive role of dopant N and the ideal double layer capacitor nature with a charge/discharge process. However, the quinine/hydroquinone redox peaks still existed in AG after KOH activation as shown in Figure 5(A(c)). In addition, a largely increased peak area of AG is observed compared with that of RGO due to the increased rough structure increased surface area, indicating the positive role

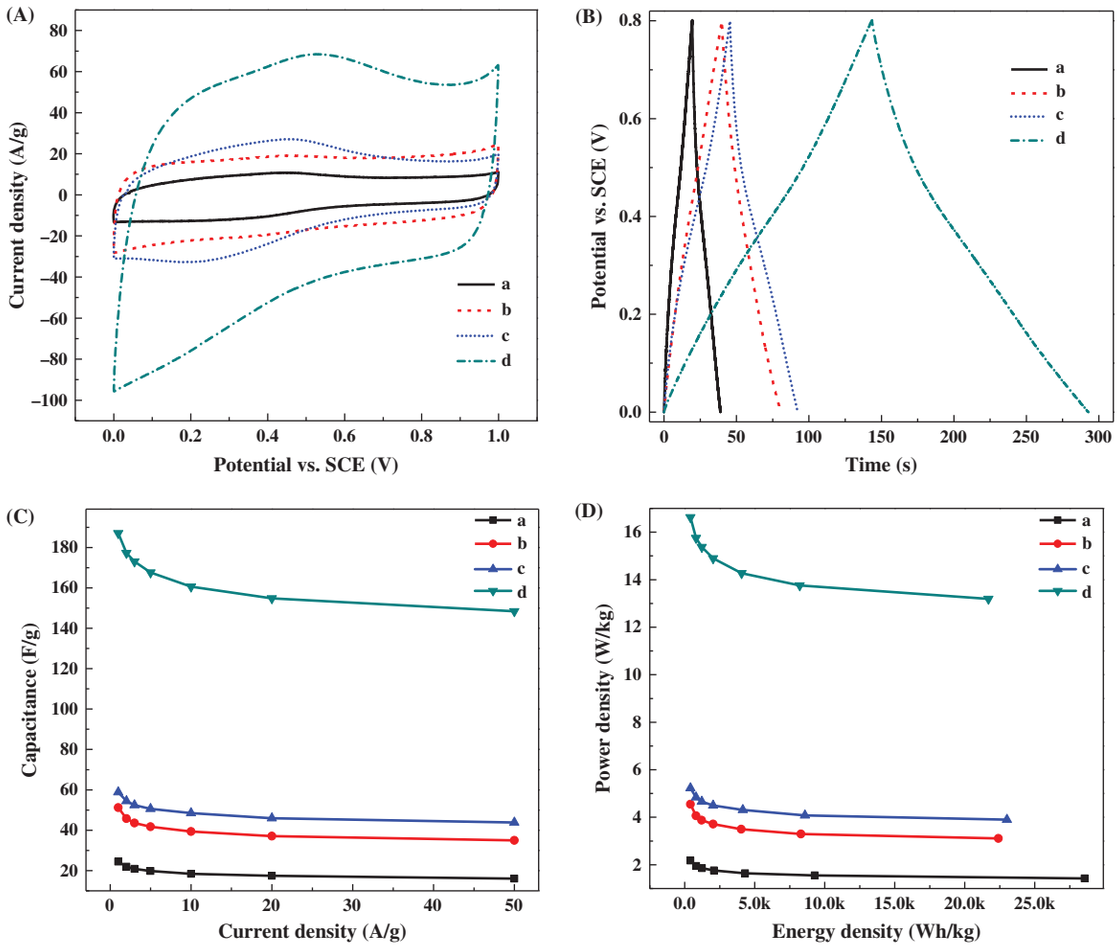

Fig. 5. (A) CV conducted at a scan rate of 500 mV/s and (B) charge–discharge with a current density as 1 A/g, (C) specific capacitance dependence on current density and (D) ragone plot of (a) RGO, (b) N-G, (c) AG and (d) N-AG measured in 1.0 M H_2SO_4 aqueous solution, the data is normalized to the mass of graphene.

of KOH activation. For N-AG, Figure 4(A(d)), depressed quinine/hydroquinone peaks were observed due to the introduced N-defects. Obviously, it is clearly seen from Figure 5(A) that the N-AG exhibits a much higher current density than other graphene counterparts, suggesting that N-AG is the most promising materials as supercapacitor electrodes among all the samples.

Galvanostatic charge–discharge (GCD) as a reliable method for measuring the specific capacitance of supercapacitor were also conducted in the same H_2SO_4 solution from 0 to 0.8 V with a current density as 1 A/g as shown in Figure 5(B). The increase in the discharging time always represents a higher capacitance. It is obtained that the capacitance of graphene can be greatly enhanced through the KOH activation and the N doping as confirmed by the discharging time order as RGO < N-G < AG < N-AG. The specific capacitances of the different graphene samples calculated from the CV at 500 mV/s and the charge–discharge at 1 A/g are summarized in Table II, the capacitance values observed in CV and C–d curves follow the same order as N-AG > AG > N-G > RGO, confirming the positive roles of KOH activation and N-doping respectively. Furthermore, the correlation between the specific capacitance and the current density for these four graphene samples is also presented in Figure 5(C). The N-AG has the highest capacity among all samples at all the same scan rate. For instance, the N-AG possess a specific capacitance of approaching 186.63 F/g with 1 A/g current density, which is three and four times higher than the specific capacity for AG (58.38 F/g) and N-G (24.25 F/g),

Table II. Summary of capacitance, energy density and power density values of different graphenes calculated for CV and GCD results.

Graphene	CV C_s 500 mV/s (F/g)	C–d C_s 1 A/g (F/g)	Energy density (Wh/kg)	Power density (W/kg)
RGO	16.30	24.25	2.16	404.25
N-G	34.63	50.88	4.52	397.05
AG	37.86	58.38	5.19	403.54
N-AG	104.21	186.63	16.59	399.22

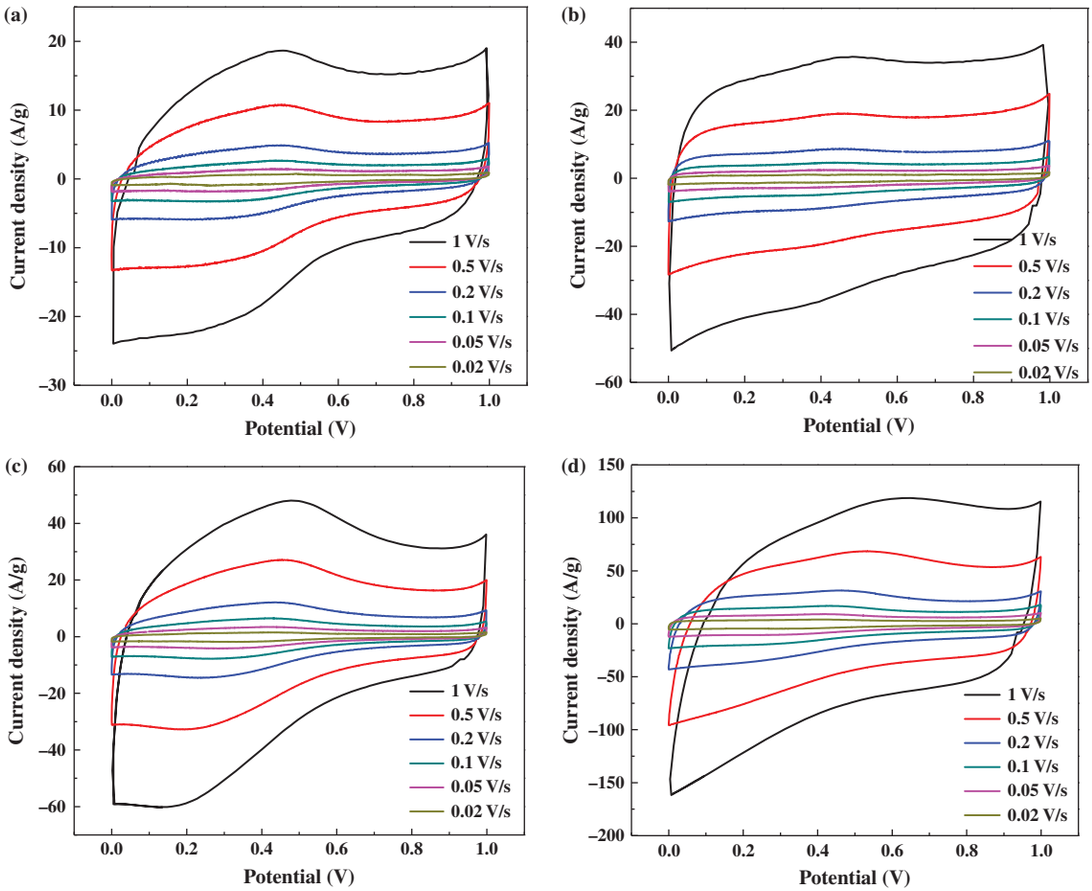

Fig. 6. CV curves of (a) RGO, (b) N-G, (c) PG and (d) N-PG in 1.0 M H_2SO_4 with different scan rate ranging from 0.02 to 1 V/s.

respectively. Notably, the capacitance shows almost nine times larger than that of RGO (24.25 F/g), indicating a dramatic capacitance increase when combining KOH activation with N-doping processes. Furthermore, the N-AG shows a capacity of 186.63 F/g and 154.33 F/g with 1 and 50 A/g current density, respectively, suggesting a good rate capability for N-AG supercapacitors. In addition, the voltage drop at the initiation of the discharge is extremely small of N-AG among all the graphene, indicating a very low equivalent series resistance (ESR) in the supercapacitor and the potential of N-AG for high-power operations. The improvement in power density of N-AG is further confirmed by the Ragone plot of these four graphene as shown in Figure 5(D). Similar power density trend was clearly observed as N-AG > AG > N-G > RGO with similar range of energy density. The as-developed N-AG also outperform graphene reported previously and is also even comparable to those of metal oxide/graphene and polymer/graphene composites in terms of capacitance and energy density.[103–107] It should be noted that, besides the appealing electrochemical properties as supercapacitor, the facile prepared N-AG may also show considerable performances regarding oxygen reduction reaction (ORR) and Li-ion batteries, which is pivotal to its wide practical applications.

3.2.2. EIS Characterization

Electrochemical impedance spectroscopy (EIS) as a power technique to obtain a further fundamental understanding of the inherent reaction kinetics of the electrode materials was also employed, Figure 7 presents the semicircular Nyquist plots of imaginary (Z'' Ω) versus real (Z' Ω) components of impedance conducted in the frequency range of 100,000 to 0.01 Hz with a 5 mV amplitude referring to open potential in 1.0 M H_2SO_4, the enlarged part of the high frequency region is also provided, No resistor-capacitor (RC) loops or semicircles appear in the high frequency region, indicating a negligible charge resistance.[108] The excellent capacitance performance can be clearly demonstrated with the graphene electrode approaching an almost vertical line. It is clearly seen from the enlarged high frequency part that the slope of the graphene samples follow an order as N-AG > AG > N-G > RGO, demonstrating enhanced reaction kinetics due to the KOH activation and N doping and is also in good consistent with the CV and GCD analysis. In order to further analyze the EIS

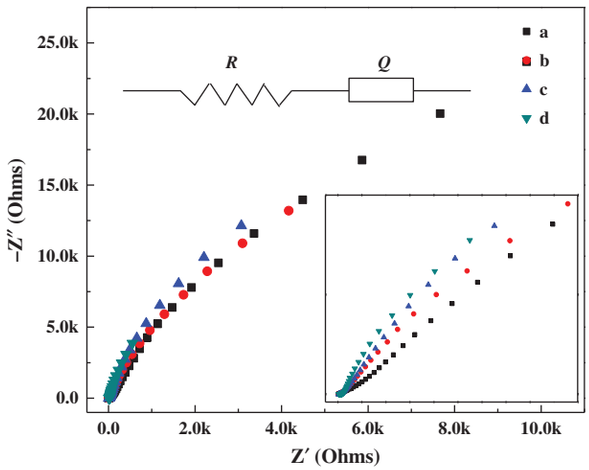

Fig. 7. Nyquist plot of (a) RGO, (b) N-G, (c) AG and (d) N-AG, respectively. The inset is the enlarged part of high frequency region.

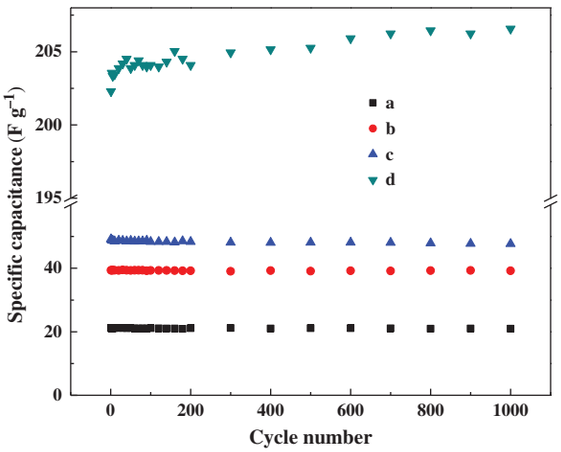

Fig. 8. Cycling performance as a function of cycling number at a current density of 1 A/g for (a) RGO, (b) N-G, (c) AG and (d) N-AG, respectively.

behavior comprehensively and deeply, simulations are performed on the basis of the equivalent-circuit model using ZsimpWin commercial software based on an equivalent electric circuit as shown inset of Figure 7. The simulated results and associated % error are provide in Table III. Almost same *R* values are clearly obtained due to the same solution resistance. Furthermore, it is clearly observed that the *Q* value increased monotonously as N-AG > AG > N-G > RGO, indicating the same energy storage trend after KOH activation and N-doping.

3.2.3. Cycling Performance

Since a long cycling performance is among the most important criteria for supercapacitors, the cycling performance is conducted using GCD for 1000 cycles with a current density of 1 A/g. The cycling performances with specific capacitances are shown in Figure 8. It is clearly seen that all the graphene electrodes exhibit excellent performance due to the charging mechanisms of ultracapacitors. All the capacitances have a great retention after 1000 cycles and follow the same order as initial capacitances. However, an obvious capacitance increase is clearly seen for N-AG due to the electro-activation, which implies its great potential application as supercapacitor materials due to this comparable capacitance as that of pesudocapacitors and the excellent cycling performance, highlighting that N-AG have an excellent electrochemical stability and a high degree of reversibility. The above results clearly reveal that the electrochemical performance of graphene can be greatly enhanced combining KOH activation and nitrogen doping processes.

Table III. Impedance components for different electrodes by fitting the experimental data using Zsimp-Win software based on the equivalent circuit presented inset of Figure 5.

	R/Ω		Q/C		n	
Electrode	Value	Error %	Value	Error %	Value	Error %
RGO	5.504	1.907	0.00042	1.675	0.8219	0.517
N-G	5.402	2.293	0.00089	2.25	0.8556	0.7615
AG	8.193	3.46	0.00102	3.57	0.855	1.309
N-AG	11.11	4.558	0.00331	5.443	0.8476	2.481

4. CONCLUSIONS

A facile hydrothermal synthesis method combining KOH activation and N-doping was successfully employed to synthesis nitrogen doped activated graphene, which is economically and effectively at a very high yield, implying feasibility for mass production. The synthesized N-AG exhibited relatively decreased oxygen containing groups with increased defects due to the etching nature of KOH and N containing defects were also introduced with this effective N doping method. These unique properties endow them as a promising electrode for supercapacitors with high capacity, excellent rate capability, and long-term stability. Due to the possibility of scalable synthesis and prominent properties, the N-AG can offer attractive opportunities for both fundamental study and potential industrial applications in catalysis, adsorption, energy storage, and energy conversion systems.

References and Notes

1. M. Sevilla, L. Yu, L. Zhao, C. O. Ania, and M.-M. Titiricic, Surface modification of CNTs with N-doped carbon: An effective way of enhancing their performance in supercapacitors. *ACS Sustainable Chemistry and Engineering* 2, 1049 (**2014**).
2. X. Luo, J. Wang, M. Dooner, and J. Clarke, Overview of current development in electrical energy storage technologies and the application potential in power system operation. *Applied Energy* 137, 511 (**2015**).
3. C. Cheng, R. Fan, Z. Wang, Q. Shao, X. Guo, P. Xie, Y. Yin, Y. Zhang, L. An, and Y. Lei, Tunable and weakly negative permittivity in carbon/silicon nitride composites with different carbonizing temperatures. *Carbon* 125, 103 (**2017**).

4. Z. Zhang, Z. Zhou, H. Peng, Y. Qin, and G. Li, Nitrogen-and oxygen-containing hierarchical porous carbon frameworks for high-performance supercapacitors. *Electrochim. Acta* 134, 471 (**2014**).
5. C. Lin, L. Hu, C. Cheng, K. Sun, X. Guo, Q. Shao, J. Li, N. Wang, and Z. Guo, Nano-$TiNb_2O_7$/carbon nanotubes composite anode for enhanced lithium-ion storage. *Electrochim. Acta* 260, 65 (**2018**).
6. X. Lou, C. Lin, Q. Luo, J. Zhao, B. Wang, J. Li, Q. Shao, X. Guo, N. Wang, and Z. Guo, Crystal structure modification enhanced $FeNb_{11}O_{29}$ anodes for lithium-ion batteries. *ChemElectroChem.* 4, 3171 (**2017**).
7. K.-L. Chiu and W.-S. Chen, Recovery and separation of valuable metals from cathode materials of spent lithium-ion batteries (LIBs) by ion exchange. *Sci. Adv. Mater.* 9, 2155 (**2017**).
8. H. Wei, H. Gu, J. Guo, X. Yan, J. Liu, D. Cao, X. Wang, S. Wei, and Z. Guo, *Adv. Compos. Hybrid Mater.* 1, 127 (**2018**).
9. F. Ran, X. Yang, and L. Shao, Recent progress in carbon-based nanoarchitectures for advanced supercapacitors. *Adv. Compos. Hybrid Mater.* 1, 32 (**2018**).
10. Z. Wu, S. Gao, L. Chen, D. Jiang, Q. Shao, B. Zhang, Z. Zhai, C. Wang, M. Zhao, and Y. Ma, Electrically insulated epoxy nanocomposites reinforced with synergistic core–shell SiO_2@MWCNTs and montmorillonite bifillers. *Macromol. Chem. Phys.* 218 (**2017**).
11. J. Chen, C. Li, and G. Shi, Graphene materials for electrochemical capacitors. *The Journal of Physical Chemistry Letters* 4, 1244 (**2013**).
12. C. Kim, G.-W. Yoo, and J.-T. Son, Synthesis and electrochemical properties of $0.5LiFePO_4$–$0.5Li_2FeSiO_4$ cathode material for lithium-ion batteries. *Sci. Adv. Mater.* 9, 771 (**2017**).
13. X. Guan, G. Zheng, K. Dai, C. Liu, X. Yan, C. Shen, and Z. Guo, Carbon nanotubes-adsorbed electrospun PA66 nanofiber bundles with improved conductivity and robust flexibility. *ACS Applied Materials and Interfaces* 8, 14150 (**2016**).
14. Q. Hou, J. Ren, H. Chen, P. Yang, Q. Shao, M. Zhao, X. Zhao, H. He, N. Wang, Q. Luo, and Z. Guo, Synergistic hematite-fullerene electron-extracting layers for improved efficiency and stability in perovskite solar cells. *Chemelectrochem.* 5, 726 (**2018**).
15. P. Kossyrev, Carbon black supercapacitors employing thin electrodes. *J. Power Sources* 201, 347 (**2012**).
16. Y. Gao, Y. S. Zhou, M. Qian, X. N. He, J. Redepenning, P. Goodman, H. M. Li, L. Jiang, and Y. F. Lu, Chemical activation of carbon nano-onions for high-rate supercapacitor electrodes. *Carbon* 51, 52 (**2013**).
17. S. W. Lee, J. S. Kang, H. R. Lee, and K. C. Park, Structural properties of carbon nanotube electron beam (C-Beam) crystallization silicon thin films. *Sci. Adv. Mater.* 9, 962 (**2017**).
18. K. Zhang, G.-H. Li, L.-M. Feng, N. Wang, J. Guo, K. Sun, K.-X. Yu, J.-B. Zeng, T. Li, and Z. Guo, Ultralow percolation threshold and enhanced electromagnetic interference shielding in poly(l-lactide)/multi-walled carbon nanotube nanocomposites with electrically conductive segregated networks. *Journal of Materials Chemistry C* 5, 9359 (**2017**).
19. J. Zhao, L. Wu, C. Zhan, Q. Shao, Z. Guo, and L. Zhang, Overview of polymer nanocomposites: Computer simulation understanding of physical properties. *Polymer* 133, 272 (**2017**).
20. B. Kim, H. Chung, and W. Kim, High-performance supercapacitors based on vertically aligned carbon nanotubes and nonaqueous electrolytes. *Nanotechnology* 23, 155401 (**2012**).
21. Z. Fang, H. Yu, Y. Dang, N. Gao, N. Ma, J. Peng, K. Xie, and L. Li, Electrochemical and printable properties of polydopamine decorated carbon nanotube ink. *Sci. Adv. Mater.* 9, 2039 (**2017**).
22. L.-F. Chen, X.-D. Zhang, H.-W. Liang, M. Kong, Q.-F. Guan, P. Chen, Z.-Y. Wu, and S.-H. Yu, Synthesis of nitrogen-doped porous carbon nanofibers as an efficient electrode material for supercapacitors. *ACS Nano* 6, 7092 (**2012**).
23. Y.-H. Hsu, C.-C. Lai, C.-L. Ho, and C.-T. Lo, Preparation of interconnected carbon nanofibers as electrodes for supercapacitors. *Electrochim. Acta* 127, 369 (**2014**).
24. Y. He, S. Yang, H. Liu, Q. Shao, Q. Chen, C. Lu, Y. Jiang, C. Liu, and Z. Guo, Reinforced carbon fiber laminates with oriented carbon nanotube epoxy nanocomposites: Magnetic field assisted alignment and cryogenic temperature mechanical properties. *J. Colloid Interface Sci.* 517, 40 (**2018**).
25. H. M. Jeong, J. W. Lee, W. H. Shin, Y. J. Choi, H. J. Shin, J. K. Kang, and J. W. Choi, Nitrogen-doped graphene for high-performance ultracapacitors and the importance of nitrogen-doped sites at basal planes. *Nano Lett.* 11, 2472 (**2011**).
26. Y. Liu, J. Manuel, X. Zhao, A. K. Haridas, G. S. Chauhan, J.-K. Kim, K.-K. Cho, H.-J. Ahn, and J.-H. Ahn, Effect of carbon coating and magnesium doping on electrochemical properties of $LiFePO_4$ for lithium ion batteries. *Sci. Adv. Mater.* 9, 1266 (**2017**).
27. H. Wang, Z. Xu, H. Yi, H. Wei, Z. Guo, and X. Wang, One-step preparation of single-crystalline Fe_2O_3 particles/graphene composite hydrogels as high performance anode materials for supercapacitors. *Nano Energy* 7, 86 (**2014**).
28. Y. Jiang, P. Wang, X. Zang, Y. Yang, A. Kozinda, and L. Lin, Uniformly embedded metal oxide nanoparticles in vertically aligned carbon nanotube forests as pseudocapacitor electrodes for enhanced energy storage. *Nano Lett.* 13, 3524 (**2013**).
29. J. Zhang, S. Liu, C. Yan, X.-J. Wang, L. Wang, Y.-M. Yu, and S.-Y. Li, Abrasion properties of self-suspended hairy titanium dioxide nanomaterials. *Applied Nanoscience* 7, 691 (**2017**).
30. T. Kim, K. Jang, C. P. T. Nguyen, J. Raja, S. Kang, S. Lee, T. T. Trinh, J. Jung, Y.-J. Lee, and J. Yi, Improvement of electrical characteristics of a-InSnZnO TFT using hydrogenated gate dielectric. *Sci. Adv. Mater.* 9, 924 (**2017**).
31. R. Aparna, R. Prasad, and N. P. Nirmal, An injectable *in-situ* conducting thermosensitive gel for controlled delivery of vancomycin in osteomyelitis treatment and bone regeneration. *Sci. Adv. Mater.* 8, 1470 (**2016**).
32. Y. Zhao, H. Wei, M. Arowo, X. Yan, W. Wu, J. Chen, Y. Wang, and Z. Guo, Electrochemical energy storage by polyaniline nanofibers: High gravity assisted oxidative polymerization versus rapid mixing chemical oxidative polymerization. *PCCP* 17, 1498 (**2015**).
33. H. Liu, Y. Li, K. Dai, G. Zheng, C. Liu, C. Shen, X. Yan, J. Guo, and Z. Guo, Electrically conductive thermoplastic elastomer nanocomposites at ultralow graphene loading levels for strain sensor applications. *Journal of Materials Chemistry C* 4, 157 (**2016**).
34. Y. Zheng, Y. Zheng, S. Yang, Z. Guo, T. Zhang, H. Song, and Q. Shao, Esterification synthesis of ethyl oleate catalyzed by Brønsted acid-surfactant-combined ionic liquid. *Green Chemistry Letters and Reviews* 10, 202 (**2017**).
35. H. Wei, Y. Wang, J. Guo, X. Yan, R. O'Connor, X. Zhang, N. Z. Shen, B. L. Weeks, X. Huang, and S. Wei, Electropolymerized polypyrrole nanocoatings on carbon paper for electrochemical energy storage. *ChemElectroChem.* 2, 119 (**2015**).
36. V. Augustyn, P. Simon, and B. Dunn, Pseudocapacitive oxide materials for high-rate electrochemical energy storage. *Energy and Environmental Science* 7, 1597 (**2014**).
37. G.-W. Yoo, B.-C. Jang, C. Kim, and J.-T. Son, The effect of surface coating on $LiNi_{0.6}Co_{0.1}Mn_{0.3}O_2$ cathode material for lithium secondary battery by PEDOT-PEG block copolymer. *Sci. Adv. Mater.* 9, 790 (**2017**).
38. H.-J. Jeon, G.-W. Yoo, C. Kim, B.-C. Jang, S.-B. Yang, and J.-T. Son, Functionality of sugar coated for $Li[Li_{0.2}Ni_{0.2}Co_{0.08}Mn_{0.52}]O_2$ as positive electrode materials for lithium-ion secondary batteries. *Sci. Adv. Mater.* 9, 824 (**2017**).
39. K. Kai, Y. Kobayashi, Y. Yamada, K. Miyazaki, T. Abe, Y. Uchimoto, and H. Kageyama, Electrochemical characterization of single-layer MnO_2 nanosheets as a high-capacitance pseudocapacitor electrode. *J. Mater. Chem.* 22, 14691 (**2012**).

ARTICLE

40. G. A. Snook, P. Kao, and A. S. Best, Conducting-polymer-based supercapacitor devices and electrodes. *J. Power Sources* 196, 1 (**2011**).

41. J. Yang, T. Lan, J. Liu, Y. Song, and M. Wei, Supercapacitor electrode of hollow spherical V_2O_5 with a high pseudocapacitance in aqueous solution. *Electrochim. Acta* 105, 489 (**2013**).

42. F. Su, C. K. Poh, J. S. Chen, G. Xu, D. Wang, Q. Li, J. Lin, and X. W. Lou, Nitrogen-containing microporous carbon nanospheres with improved capacitive properties. *Energy and Environmental Science* 4, 717 (**2011**).

43. G. Lota, B. Grzyb, H. Machnikowska, J. Machnikowski, and E. Frackowiak, Effect of nitrogen in carbon electrode on the supercapacitor performance. *Chem. Phys. Lett.* 404, 53 (**2005**).

44. C. Mao, Y. Zhu, and W. Jiang, Design of electrical conductive composites: Tuning the morphology to improve the electrical properties of graphene filled immiscible polymer blends. *ACS Applied Materials and Interfaces* 4, 5281 (**2012**).

45. S. Vadivel, J. Theerthagiri, J. Madhavan, and D. Maruthamani, Synthesis of polyaniline/graphene oxide composite via ultrasonication method for photocatalytic applications. *Mater. Focus* 5, 393 (**2016**).

46. B. Song, T. Wang, H. Sun, Q. Shao, J. Zhao, K. Song, L. Hao, L. Wang, and Z. Guo, Two-step hydrothermally synthesized carbon nanodots/WO_3 photocatalysts with enhanced photocatalytic performance. *Dalton Transactions* 46, 15769 (**2017**).

47. J. Huang, Y. Cao, Q. Shao, X. Peng, and Z. Guo, Magnetic nanocarbon adsorbents with enhanced hexavalent chromium removal: Morphology dependence of fibrillar versus particulate structures. *Industrial and Engineering Chemistry Research* 56, 10689 (**2017**).

48. C. Hu, Z. Li, Y. Wang, J. Gao, K. Dai, G. Zheng, C. Liu, C. Shen, H. Song, and Z. Guo, Comparative assessment of the strain-sensing behaviors of polylactic acid nanocomposites: Reduced graphene oxide or carbon nanotubes. *Journal of Materials Chemistry C* 5, 2318 (**2017**).

49. A. K. Geim, and K. S. Novoselov, The rise of graphene. *Nat. Mater.* 6, 183 (**2007**).

50. H. Liu, W. Huang, X. Yang, K. Dai, G. Zheng, C. Liu, C. Shen, X. Yan, J. Guo, and Z. Guo, Organic vapor sensing behaviors of conductive thermoplastic polyurethane–graphene nanocomposites. *Journal of Materials Chemistry C* 4, 4459 (**2016**).

51. Y. Li, B. Zhou, G. Zheng, X. Liu, T. Li, C. Yan, C. Cheng, K. Dai, C. Liu, and C. Shen, Continuously prepared highly conductive and stretchable SWNT/MWNT synergistically composited electrospun thermoplastic polyurethane yarns for wearable sensing. *J. Mater. Chem. C* 6, 2258 (**2018**).

52. J.-X. Zhang, Y.-X. Liang, X. Wang, H.-J. Zhou, S.-Y. Li, J. Zhang, Y. Feng, N. Lu, Q. Wang, and Z. Guo, Strengthened epoxy resin with hyperbranched polyamine-ester anchored graphene oxide via novel phase transfer approach. *Adv. Compos. Hybrid Mater.* (**2017**).

53. J.-X. Zhang, K.-M. Jang, Y.-P. Zheng, F. Wu, and Y.-Q. Li, The preparation of solvent-free multiwall carbon nanotubes/silica hybrid nanomaterial with liquid-like behavior. *Functional Materials Letters* 6, 1350015 (**2013**).

54. J. Zhang, Y. Zheng, H. Zhou, J. Zhang, and J. Zou, The influence of hydroxylated carbon nanotubes on epoxy resin composites. *Advances in Materials Science and Engineering* 2012, 518392 (**2012**).

55. S. Kim, K. H. Kim, and C. W. Bark, Two-dimensional nanomaterials: Their structures, synthesis, and applications. *Sci. Adv. Mater.* 9, 1441 (**2017**).

56. J. Song, J. Zhang, and C. Lin, Influence of graphene oxide on the tribological and electrical properties of PMMA composites. *Journal of Nanomaterials* 2013, 84 (**2013**).

57. T. Kim, U. J. Kim, H. B. Son, and J. Hur, Investigation on the ion-gel dielectric characteristics for graphene transistor toward flexible and transparent devices. *Sci. Adv. Mater.* 9, 1589 (**2017**).

58. M. Park, K. C. Kwon, J. H. Oh, Y. G. Kim, H. W. Jang, and S. Y. Kim, Effect of fluoropolymer assisted transfer on graphene doping. *Sci. Adv. Mater.* 9, 758 (**2017**).

59. K. Zhu, T. Jiao, L. Zhang, R. Xing, R. Guo, J. Zhou, C. Hou, Q. Zhang, Q. Peng, and X. Li, Preparation and absorption capacity evaluation of composite hydrogels via graphene oxide and multi-amine molecules. *Sci. Adv. Mater.* 8, 1400 (**2016**).

60. Z. Hu, C. Wang, F. Zhao, X. Xu, S. Wang, L. Yu, D. Zhang, and Y. Huang, Fabrication of a graphene/C_{60} nanohybrid via γ-cyclodextrin host–guest chemistry for photodynamic and photothermal therapy. *Nanoscale* 9, 8825 (**2017**).

61. Z. Sun, L. Zhang, F. Dang, Y. Liu, Z. Fei, Q. Shao, H. Lin, J. Guo, L. Xiang, and N. Yerra, Experimental and simulation-based understanding of morphology controlled barium titanate nanoparticles under co-adsorption of surfactants. *CrystEngComm.* 19, 3288 (**2017**).

62. L. Zhang, W. Yu, C. Han, J. Guo, Q. Zhang, H. Xie, Q. Shao, Z. Sun, and Z. Guo, Large scaled synthesis of heterostructured electrospun TiO_2/SnO_2 nanofibers with an enhanced photocatalytic activity. *J. Electrochem. Soc.* 164, H651 (**2017**).

63. L. Zhang, M. Qin, W. Yu, Q. Zhang, H. Xie, Z. Sun, Q. Shao, X. Guo, L. Hao, and Y. Zheng, Heterostructured TiO_2/WO_3 nanocomposites for photocatalytic degradation of toluene under visible light. *J. Electrochem. Soc.* 164, H1086 (**2017**).

64. A. K. Geim, Graphene: Status and prospects. *Science* 324, 1530 (**2009**).

65. Z. Hu, D. Zhang, L. Yu, and Y. Huang, Light-triggered C_{60} release from a graphene/cyclodextrin nanoplatform for the protection of cytotoxicity induced by nitric oxide. *Journal of Materials Chemistry B* 6, 518 (**2018**).

66. Z. Wen, X. Wang, S. Mao, Z. Bo, H. Kim, S. Cui, G. Lu, X. Feng, and J. Chen, Crumpled nitrogen-doped graphene nanosheets with ultrahigh pore volume for high-performance supercapacitor. *Adv. Mater.* 24, 5610 (**2012**).

67. D. Chen, L. Tang, and J. Li, Graphene-based materials in electrochemistry. *Chem. Soc. Rev.* 39, 3157 (**2010**).

68. H. Liu, M. Dong, W. Huang, J. Gao, K. Dai, J. Guo, G. Zheng, C. Liu, C. Shen, and Z. Guo, Lightweight conductive graphene/thermoplastic polyurethane foams with ultrahigh compressibility for piezoresistive sensing. *Journal of Materials Chemistry C* 5, 73 (**2017**).

69. C. Wang, M. Zhao, J. Li, J. Yu, S. Sun, S. Ge, X. Guo, F. Xie, B. Jiang, and E. K. Wujcik, Silver nanoparticles/graphene oxide decorated carbon fiber synergistic reinforcement in epoxy-based composites. *Polymer* 131, 263 (**2017**).

70. Z. Hu, Q. Shao, M. G. Moloney, X. Xu, D. Zhang, J. Li, C. Zhang, and Y. Huang, Nondestructive functionalization of graphene by surface-initiated atom transfer radical polymerization: An ideal nanofiller for poly (p-phenylene benzobisoxazole) fibers. *Macromolecules* 50, 1422 (**2017**).

71. V. M. Pereira, A. C. Neto, H. Liang, and L. Mahadevan, Geometry, mechanics, and electronics of singular structures and wrinkles in graphene. *Phys. Rev. Lett.* 105, 156603 (**2010**).

72. H. D. Lim, B. K. Kang, S. N. Tiruneh, and D. H. Yoon, Hollow reduced graphene oxide-NiCo hydroxide nanowall hydrid structure for high-performance supercapacitor. *Sci. Adv. Mater.* 9, 1241 (**2017**).

73. X. Wang, X. Liu, H. Yuan, H. Liu, C. Liu, T. Li, C. Yan, X. Yan, C. Shen, and Z. Guo, Non-covalently functionalized graphene strengthened poly(vinyl alcohol). *Mater. Des.* 139, 372 (**2018**).

74. G. Goncalves, P. A. Marques, C. M. Granadeiro, H. I. Nogueira, M. Singh, and J. Gracio, Surface modification of graphene nanosheets with gold nanoparticles: The role of oxygen moieties at graphene surface on gold nucleation and growth. *Chem. Mater.* 21, 4796 (**2009**).

75. L. Dai, Functionalization of graphene for efficient energy conversion and storage. *Acc. Chem. Res.* 46, 31 (**2012**).

76. H. Song, M. Wang, Y. Wang, Y. Zhang, A. Umar, and Z. Guo, Waterborne polyurethane/graphene oxide nanocomposites with enhanced properties. *Sci. Adv. Mater.* 9, 1895 **(2017)**.

77. J. Han, L. L. Zhang, S. Lee, J. Oh, K.-S. Lee, J. R. Potts, J. Ji, X. Zhao, R. S. Ruoff, and S. Park, Generation of B-doped graphene nanoplatelets using a solution process and their supercapacitor applications. *ACS Nano* 7, 19 **(2012)**.

78. F. Razmjooei, K. P. Singh, M. Y. Song, and J.-S. Yu, Enhanced electrocatalytic activity due to additional phosphorous doping in nitrogen and sulfur-doped graphene: A comprehensive study. *Carbon* 78, 257 **(2014)**.

79. C. Rao, K. Gopalakrishnan, and A. Govindaraj, Synthesis, properties and applications of graphene doped with boron, nitrogen and other elements. *Nano Today* 9, 324 **(2014)**.

80. X. Wang, G. Sun, P. Routh, D.-H. Kim, W. Huang, and P. Chen, Heteroatom-doped graphene materials: Syntheses, properties and applications. *Chem. Soc. Rev.* 43, 7067 **(2014)**.

81. D. Geng, Y. Chen, Y. Chen, Y. Li, R. Li, X. Sun, S. Ye, and S. Knights, High oxygen-reduction activity and durability of nitrogen-doped graphene. *Energy and Environmental Science* 4, 760 **(2011)**.

82. H. Wang, C. Zhang, Z. Liu, L. Wang, P. Han, H. Xu, K. Zhang, S. Dong, J. Yao, and G. Cui, Nitrogen-doped graphene nanosheets with excellent lithium storage properties. *J. Mater. Chem.* 21, 5430 **(2011)**.

83. H. Wang, T. Maiyalagan, and X. Wang, Review on recent progress in nitrogen-doped graphene: Synthesis, characterization, and its potential applications. *ACS Catalysis* 2, 781 **(2012)**.

84. N. P. Wickramaratne, J. Xu, M. Wang, L. Zhu, L. Dai, and M. Jaroniec, Nitrogen enriched porous carbon spheres: Attractive materials for supercapacitor electrodes and CO_2 adsorption. *Chem. Mater.* 26, 2820 **(2014)**.

85. Y. Zhu, S. Murali, M. D. Stoller, K. Ganesh, W. Cai, P. J. Ferreira, A. Pirkle, R. M. Wallace, K. A. Cychosz, and M. Thommes, Carbon-based supercapacitors produced by activation of graphene. *Science* 332, 1537 **(2011)**.

86. J. Wang and S. Kaskel, KOH activation of carbon-based materials for energy storage. *J. Mater. Chem.* 22, 23710 **(2012)**.

87. E. Raymundo-Pinero, P. Azais, T. Cacciaguerra, D. Cazorla-Amorós, A. Linares-Solano, and F. Béguin, KOH and NaOH activation mechanisms of multiwalled carbon nanotubes with different structural organisation. *Carbon* 43, 786 **(2005)**.

88. K. Kierzek, E. Frackowiak, G. Lota, G. Gryglewicz, and J. Machnikowski, Electrochemical capacitors based on highly porous carbons prepared by KOH activation. *Electrochim. Acta* 49, 515 **(2004)**.

89. D. Lozano-Castello, M. Lillo-Rodenas, D. Cazorla-Amorós, and A. Linares-Solano, Preparation of activated carbons from Spanish anthracite: I. activation by KOH. *Carbon* 39, 741 **(2001)**.

90. H. Marsh, D. S. Yan, T. M. O'Grady, and A. Wennerberg, Formation of active carbons from cokes using potassium hydroxide. *Carbon* 22, 603 **(1984)**.

91. J. Maciá-Agulló, B. Moore, D. Cazorla-Amorós, and A. Linares-Solano, Activation of coal tar pitch carbon fibres: Physical activation versus chemical activation. *Carbon* 42, 1367 **(2004)**.

92. T. Kim, G. Jung, S. Yoo, K. S. Suh, and R. S. Ruoff, Activated graphene-based carbons as supercapacitor electrodes with macro- and mesopores. *ACS Nano* 7, 6899 **(2013)**.

93. W. S. Hummers and R. E. Offeman, Preparation of graphitic oxide. *J. Am. Chem. Soc.* 80, 1339 **(1958)**.

94. J. Zhu, M. Chen, H. Qu, X. Zhang, H. Wei, Z. Luo, H. A. Colorado, S. Wei, and Z. Guo, Interfacial polymerized polyaniline/graphite oxide nanocomposites toward electrochemical energy storage. *Polymer* 53, 5953 **(2012)**.

95. T. Mohiuddin, A. Lombardo, R. Nair, A. Bonetti, G. Savini, R. Jalil, N. Bonini, D. Basko, C. Galiotis, and N. Marzari, Uniaxial strain in graphene by Raman spectroscopy: G peak splitting, Grüneisen parameters, and sample orientation. *Physical Review B* 79, 205433 **(2009)**.

96. Y. Liu, D. Zhang, Y. Shang, and C. Guo, A simple and efficient electrochemical reductive method for graphene oxide. *Bull. Mater. Sci.* 37, 1529 **(2014)**.

97. Y. Shao, S. Zhang, M. H. Engelhard, G. Li, G. Shao, Y. Wang, J. Liu, I. A. Aksay, and Y. Lin, Nitrogen-doped graphene and its electrochemical applications. *J. Mater. Chem.* 20, 7491 **(2010)**.

98. C. Zhang, R. Hao, H. Liao, and Y. Hou, Synthesis of amino-functionalized graphene as metal-free catalyst and exploration of the roles of various nitrogen states in oxygen reduction reaction. *Nano Energy* 2, 88 **(2013)**.

99. Q. Zhang, D. Jiang, L. Liu, Y. Huang, J. Long, G. Wu, Z. Wu, A. Umar, J. Guo, and X. Zhang, Effects of graphene oxide modified sizing agents on interfacial properties of carbon fibers/epoxy composites. *J. Nanosci. Nanotechnol.* 15, 9807 **(2015)**.

100. A. Ganguly, S. Sharma, P. Papakonstantinou, and J. Hamilton, Probing the thermal deoxygenation of graphene oxide using high-resolution *in situ* X-ray-based spectroscopies. *The Journal of Physical Chemistry C* 115, 17009 **(2011)**.

101. L. Zhang, L. Ji, P.-A. Glans, Y. Zhang, J. Zhu, and J. Guo, Electronic structure and chemical bonding of a graphene oxide–sulfur nanocomposite for use in superior performance lithium–sulfur cells. *PCCP* 14, 13670 **(2012)**.

102. S.-Y. Yang, K.-H. Chang, H.-W. Tien, Y.-F. Lee, S.-M. Li, Y.-S. Wang, J.-Y. Wang, C.-C. M. Ma, and C.-C. Hu, Design and tailoring of a hierarchical graphene-carbon nanotube architecture for supercapacitors. *J. Mater. Chem.* 21, 2374 **(2011)**.

103. S. Vivekchand, C. S. Rout, K. Subrahmanyam, A. Govindaraj, and C. Rao, Graphene-based electrochemical supercapacitors. *Journal of Chemical Sciences* 120, 9 **(2008)**.

104. Y. Xu, K. Sheng, C. Li, and G. Shi, Self-assembled graphene hydrogel via a one-step hydrothermal process. *ACS Nano* 4, 4324 **(2010)**.

105. N. A. Kumar, H.-J. Choi, Y. R. Shin, D. W. Chang, L. Dai, and J.-B. Baek, Polyaniline-grafted reduced graphene oxide for efficient electrochemical supercapacitors. *ACS Nano* 6, 1715 **(2012)**.

106. Y. Wang, H. Sun, R. Zhang, S. Yu, and J. Kong, Large scale templated synthesis of single-layered graphene with a high electrical capacitance. *Carbon* 53, 245 **(2013)**.

107. B. Wang, J. Park, C. Wang, H. Ahn, and G. Wang, Mn_3O_4 nanoparticles embedded into graphene nanosheets: Preparation, characterization, and electrochemical properties for supercapacitors. *Electrochim. Acta* 55, 6812 **(2010)**.

108. C. Xiang, M. Li, M. Zhi, A. Manivannan, and N. Wu, Reduced graphene oxide/titanium dioxide composites for supercapacitor electrodes: Shape and coupling effects. *J. Mater. Chem.* 22, 19161 **(2012)**.

ARTICLE